

Research Article

Open Access



Mildly oxidized and phenol-enriched carbon nanotubes as efficient and selective electrocatalysts for the 2e⁻ oxygen reduction reaction

Giulia Tuci^{1,*}, Marco Bonechi², Andrea Rossin¹, Enrico Berretti¹, Matteo Ceppatelli^{1,3}, Lorenzo Poggini^{1,2}, Massimo Innocenti², Giuliano Giambastiani^{1,2,*}

¹Institute of Chemistry of OrganoMetallic Compounds, ICCOM-CNR, Sesto Fiorentino 50019, Florence, Italy.

²Department of Chemistry "U. Schiff" - DICUS - and INSTM Research Unit, University of Florence, Sesto Fiorentino 50019, Florence, Italy.

³LENS, European Laboratory for Non-linear Spectroscopy, Sesto Fiorentino 50019, Florence, Italy.

***Correspondence to:** Dr. Giulia Tuci, Institute of Chemistry of OrganoMetallic Compounds, ICCOM-CNR, Via Madonna del Piano 10, Sesto Fiorentino 50019, Florence, Italy. E-mail: giulia.tuci@iccom.cnr.it; Prof. Giuliano Giambastiani, Department of Chemistry "U. Schiff" - DICUS - and INSTM Research Unit, University of Florence, Via della Lastruccia 3-13, Sesto Fiorentino 50019, Florence, Italy. E-mail: giuliano.giambastiani@unifi.it

How to cite this article: Tuci, G.; Bonechi, M.; Rossin, A.; Berretti, E.; Ceppatelli, M.; Poggini, L.; Innocenti, M.; Giambastiani, G. Mildly oxidized and phenol-enriched carbon nanotubes as efficient and selective electrocatalysts for the 2e⁻ oxygen reduction reaction. *Chem. Synth.* **2025**, *5*, 66. <https://dx.doi.org/10.20517/cs.2025.05>

Received: 8 Jan 2025 **First Decision:** 28 May 2025 **Revised:** 5 Jun 2025 **Accepted:** 24 Jun 2025 **Published:** 23 Jul 2025

Academic Editor: Xiaoxin Zou **Copy Editor:** Pei-Yun Wang **Production Editor:** Pei-Yun Wang

Abstract

The electrochemical 2e⁻ oxygen reduction reaction (ORR) represents a green, cost-effective strategy towards hydrogen peroxide (H₂O₂) production other than a promising and more sustainable alternative to the currently anthraquinone-based technology. Light-weight hetero-doped carbon networks, particularly oxidized systems containing variables O-functionalities, have been deeply investigated as promising and selective metal-free electrocatalysts for the process. Following previous and positive outcomes from our team on the tailored surface engineering of complex C-nanocarbon networks with phenolic dangling groups as effective O-functionalities engaged for the molecular oxygen activation and its selective (2e⁻) electroreduction, we propose hereafter a facile, scalable and highly reproducible one-pot protocol for the mild and controlled oxidation of multi-walled carbon nanotubes. The as-prepared materials have shown a phenolic enriched surface and a superior ability to foster the almost chemoselective 2e⁻ ORR process already under low overpotential values.

Keywords: H₂O₂ electrochemical synthesis, metal-free carbon-based electrocatalysts, oxidized carbon nanotubes, 2e⁻ oxygen reduction reaction



© The Author(s) 2025. **Open Access** This article is licensed under a Creative Commons Attribution 4.0 International License (<https://creativecommons.org/licenses/by/4.0/>), which permits unrestricted use, sharing, adaptation, distribution and reproduction in any medium or format, for any purpose, even commercially, as long as you give appropriate credit to the original author(s) and the source, provide a link to the Creative Commons license, and indicate if changes were made.



INTRODUCTION

Hydrogen peroxide (H_2O_2) is a widespread, environmentally friendly oxidant whose applications span from fine chemical synthesis to paper bleaching and up to medical disinfection^[1,2]. Its global demand has reached 4.5 million metric tons in 2020 and it is expected to grow up to 5.7 million metric tons by 2027^[3]. Current technologies for H_2O_2 production mainly rely on the anthraquinone oxidation process that still suffers from many constraints such as: (1) the use of expensive platinum group metals (PGM)-based catalysts; (2) the need of centralized and large-scale infrastructures; (3) the existence of convenient and safe solutions for the H_2O_2 transportation/delivery to its ultimate destination^[4,5].

A valuable and sustainable alternative for the on-site H_2O_2 production is represented by the partial ($2e^-$) electrochemical reduction of dioxygen^[6,7]. Oxygen reduction reaction (ORR) is a multielectron process that occurs through a $2e^-$ or $4e^-$ reduction path. While a complete $4e^-$ reduction to water is widely exploited in the cathodic part of fuel cell devices^[8,9], the partial $2e^-$ reduction path can be conveniently employed for H_2O_2 electrochemical synthesis. The electrochemical $2e^-$ ORR pairs well with the urgent quest for a more and more mature transition towards *e*-catalysis^[10] where the process at standard ambient temperature and pressure (SATP) conditions can be conveniently powered by renewable (fossil fuels-free) energy sources. For these reasons, the last decade has witnessed a steadily growing interest of the scientific community for the development of electrocatalysts with improved activity and selectivity for hydrogen peroxide production with a key focus on the replacement of critical and costly metal active phases (i.e., Pt, Ag and Au)^[11,12] with cheaper and more sustainable ones. Carbon-based nanomaterials in the form of light-weight hetero-doped (i.e., N and O mainly) enriched C-networks, have recently emerged as valuable alternatives to classical (noble)-metal-based catalysts for a wide range of thermal- and electrochemical processes^[13-15], including the challenging $4e^-$ ^[16,17] and $2e^-$ ORR^[18,19]. As for the latter, carbon nanomaterials in the form of O-enriched networks seem to offer the highest performance at least in terms of process selectivity^[20-23]. In spite of a number of seminal research outcomes, a clear structure/reactivity relationship for this class of metal-free materials still remains rather elusive^[24]. Classic bulk and often batch-dependent synthetic strategies that generate O-enriched carbon samples exhibit complex morphological and chemico-physical properties, making it difficult - if not entirely speculative - to identify the nature of the active sites involved in the selective reduction process. To face this issue, we have recently proposed the C-nanomaterials engineering by tailored O-containing functional groups as a more effective synthetic tool for the control of the chemical and electronic properties of surface materials. Our evidence highlighted phenol moieties as ideal candidates for the generation of an electronic microenvironment at the C-nanomaterial surface suitable to promote the dioxygen activation and its selective electroreduction to H_2O_2 ^[25]. Although the authors are aware that electrocatalysts performance remains a complex balance between their morphology and chemical composition, the proposed top-down synthetic approach represents a powerful tool to better identify the role of O-groups in the process while driving synthetic chemists towards materials with optimized performance^[26].

In this work we have reported on two alternative, simple and easily scalable synthetic protocols for the direct surface oxidation of ultra-pure multi-walled carbon nanotubes (MWCNTs, $\geq 98\%$ in C) and their use as metal-free electrocatalysts for the selective $2e^-$ ORR. To this end, two different oxidation schemes for the bulk and multi-gram scale treatment of MWCNTs have been described and oxidation products have been thoroughly analyzed with respect to their electrocatalytic performance in the $2e^-$ ORR. In particular, MW-ox^{RT} (**1**) was prepared according to the classical sulfo-nitric acid treatment^[27,28] commonly exploited to maximize C-materials surface decoration with carboxylic moieties, while an alternative oxidation scheme based on the use of *aqua regia* was exploited to tune the O-content (oxidation degree) and relative distribution of various O-containing functionalities at the nanomaterial surface [i.e., phenolic *vs.* carboxylic

groups, MW-ox^{HT} (2)]. Our findings have unveiled that oxidation degree of C-networks did not affect linearly ORR activity whereas selectivity towards 2e⁻ ORR was largely boosted by phenol-enriched MWCNTs prepared under milder oxidation conditions based on the use of *aqua regia*.

EXPERIMENTAL

General considerations

MWCNTs (MWCNTs > 98% in C, Lot# MKBH5814V) and chemicals were provided by Merck and used as received. An Elma S15 Elmasonic sonicator bath (37 kHz) was employed for materials sonication while carbon nanotube (CNT) filtration was accomplished on polytetrafluoroethylene (PTFE) filters (Whatman®, 0.2 µm pore size) upon wetting with alcoholic solutions.

Direct surface oxidation of highly C-pure MWCNTs

A first batch of oxidized MWCNTs was prepared according to a mild (r.t.) oxidation protocol from the literature^[27]. In brief, 100 mg of MWCNTs were sonicated in 16 mL of a H₂SO₄/HNO₃ 3:1 mixture at room temperature for 24 h. Afterwards, 20 mL of distilled water were added portion-wise and the resulting suspension was collected by filtration through a PTFE membrane. The solid was then washed with distilled water and till complete neutrality of the filtering liquors. The collected oxidized sample MW-ox^{RT} (1) was then dried under vacuum to constant weight and regularly stored on air.

A second oxidation batch of MWCNTs was prepared upon a high-temperature (≈ 108 °C) treatment of the C-network with *aqua regia*. On this ground, 100 mg of MWCNTs were suspended in 16 mL of a HCl/HNO₃ 3:1 mixture (*aqua regia*) and heated overnight at the solvent temperature reflux. Afterwards, the mixture was cooled down to r.t. and treated portion-wise with 20 mL of distilled water before recovering the suspended solid by filtration through a PTFE membrane. Similarly to the above, the solid MW-ox^{HT} (2) was then washed with distilled water and till complete neutrality of the filtering liquors. The oxidized solid was finally dried under vacuum to constant weight and stored at room temperature on air.

Materials characterization and electrochemical analyses

Thermogravimetric analysis (TGA) was performed on an EXSTAR Thermo Gravimetric Analyzer Seiko 6200 in the 40-750 °C range (5 °C/min) under N₂ atmosphere (100 mL/min). Elemental analysis (EA) was accomplished by means of a Thermo FlashEA 1112 Series CHNS analyzer. Fourier-transform infrared (FT-IR) analyses were performed on a PerkinElmer Spectrum BX spectrophotometer in the 400-4,000 cm⁻¹ range and with a resolution of 1 cm⁻¹. Nitrogen physisorption analyses were conducted on a Micromeritics ASAP 2020 instrument at 77 K after degassing the samples for 24 h at 120 °C. Specific surface area (SSA) was calculated by the Brunauer-Emmet-Teller (BET) while pore size distribution was determined by Barrett-Joyner-Halenda (BJH) method. Total pore volume was estimated at $p/p_o = 0.98$ relative pressure. X-ray photoelectron spectroscopy (XPS) was performed in an ultra-high vacuum system (10⁻⁹/10⁻¹⁰ mbar). The chamber was equipped with non-monochromatized dual anode (Al and Mg) and a hemispherical electron/ion energy analyzer. The operating power of the Al X-ray source was 120 W and photoelectrons were collected normal to the sample surface, maintaining the analyzer angle in the range between analyzer axis and X-ray source fixed at 54.5°. The spectra were elaborated using CasaXPS software^[29] and peaks were deconvoluted using mixed Gaussian and Lorentzian functions. All spectra were calibrated on the basis of the C1s sp² component fixed at 284.8 eV^[25]. Samples for analyses were dispersed in ethanol upon sonication and drop cast on a gold plate to avoid any C or O contamination from the analyses support. High resolution transmission electron microscopy (TEM) was carried out on a Thermo-Fisher F200X G2 HR-TEM (200 keV beam energy). Samples were deposited on holey-carbon supported copper grids (200 mesh) by drop-casting CNT suspensions previously prepared upon sonication in isopropanol. Raman Spectra were

recorded using the 660 nm wavelength of a diode laser source, a 900 groove/mm monochromator (Acton/SpectraPro 2500i) and a N₂ cooled charge-coupled device (CCD) detector (Princeton Instruments). The beam profile was cleaned by a spatial filter and Rayleigh scattering was suppressed using holographic super notch filters. The spectral resolution was about 1 cm⁻¹[30]. The incident power was less than 1 mW and any damage of the sample due to the laser was carefully checked and excluded. Samples for analysis (i.e., pristine MWCNTs, 1 and 2) were prepared by gently pressing the fine powders into a flat thin film on glass substrate, and each material was recorded randomly on three different positions. Raman spectroscopy was employed to investigate a change in the structure during the oxidation treatments by detecting the presence and strength of D and G modes[31]. The Raman spectra showed a D band at around 1,360 cm⁻¹, and a G band at 1,590 cm⁻¹, which correspond to the presence of sp³ defects and sp² carbon atoms in the hexagonal plane of graphite-like structures, respectively. All recorded curves were baseline and fitted using Voigt line shapes, and the D- and G-peak intensities were used for the calculation of I_D/I_G ratios after background subtraction[31-33].

Electrochemical measurements were performed by means of a rotating ring-disk electrode (RRDE) from Pine Instrument Co. composed by a glassy carbon (GC) disk ($A = 0.2376 \text{ cm}^2$) and a Pt ring ($A = 0.2357 \text{ cm}^2$). All the measurements were carried out with a PGSTAT12 Autolab potentiostat/galvanostat in a three-electrodes glass cell equipped with a Pt wire and a double junction Ag/AgCl/KCl_{sat.} electrode used as counter and reference electrodes, respectively. The GC working electrode was prepared by drop-casting 3 mg (~10 µL) of the CNTs-based catalyst ink that was then allowed to dry at room temperature. The ink was prepared as follows: 10 mg of CNTs, 0.22 g of water, 0.112 g of ethanol and 0.084 g of a Nafion solution (5 wt% in lower aliphatic alcohols/water) and the mixture sonicated till obtaining a homogeneous ink (20-30 min). All measurements were performed in a N₂ or O₂ saturated 0.1 M KOH solution (pH = 13) at 10 mV/s scan rate in the +0.1 ÷ -0.9 V potential range. The Pt ring was held at +0.5 V.

H₂O₂ selectivity was estimated either from Pt ring currents [Equation (1)] of the RRDE electrode and from the average number of exchanged electrons (n) per O₂ molecule as obtained by Koutecky-Levich equation [Equation (2)]:

$$\text{H}_2\text{O}_2 (\%) = 200 * \frac{I_R/N}{I_D + I_R/N} \quad (1)$$

where I_R and I_D are the ring and the disk current values, respectively, and N is the ring collection efficiency. The latter parameter was determined experimentally using a standard K₃Fe(CN)₆ solution in KCl ($N = 0.23$).

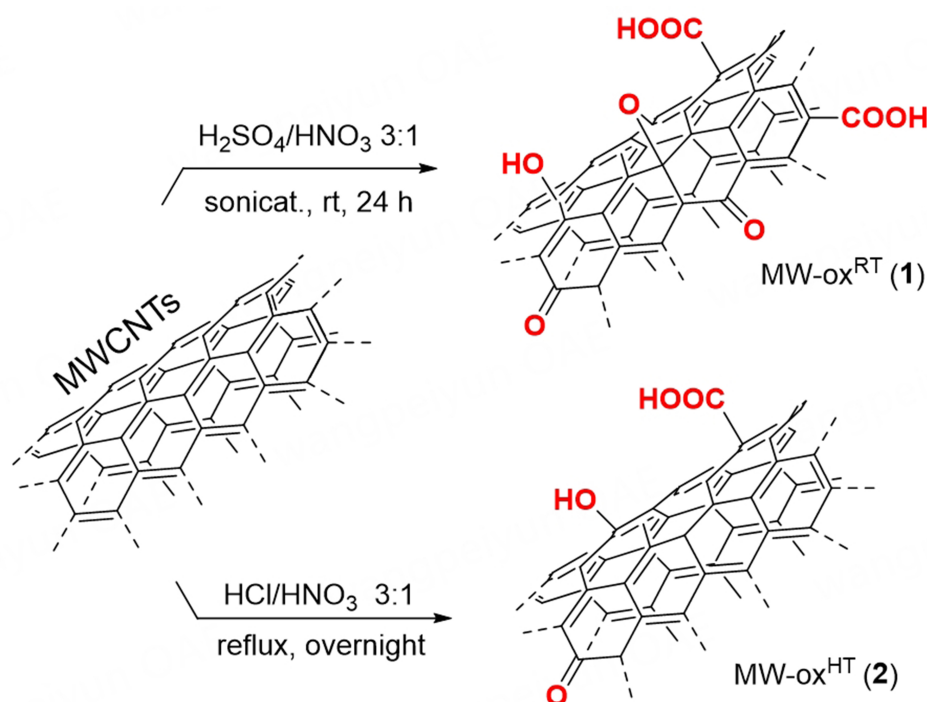
$$\frac{1}{J} = \frac{1}{J_K} + \frac{1}{nK_F\sqrt{f}} \quad \text{with } K_F = 0.2FC_0D_0^{2/3}\nu^{-1/6} \quad (2)$$

where J is the current density (mA/cm²), J_K is the kinetic current density (mA/cm²), n is the number of exchanged electrons, F is the Faraday constant, C_0 is the O₂ concentration in solution ($1.15 \times 10^{-3} \text{ mol/dm}^3$), D_0 is the oxygen diffusion coefficient ($1.95 \times 10^{-5} \text{ cm}^2/\text{s}$), ν is the electrolyte kinematic viscosity ($0.008977 \text{ cm}^2/\text{s}$) and f is the electrode angular rotation rate (rpm)[34,35]. The average number of exchanged electrons (n) was calculated from the slope of the K-L plot at -0.4 V.

RESULTS AND DISCUSSION

Synthesis of oxidized MW-ox^{RT} (1) and MW-ox^{HT} (2) samples

Two alternative, one-pot oxidation protocols have been applied to the preparation of oxidized MWCNTs [Scheme 1].



Scheme 1. Synthesis of MW-ox^{RT} (1) and MW-ox^{HT} (2).

MW-ox^{RT} (1) was prepared according to classical procedures from the literature aimed at maximizing the generation of O-containing functionalities at the nanomaterial surface^[27,28]. In particular, highly C-pure MWCNTs dispersed in a concentrated sulfuric and nitric acid mixture have been oxidized at ambient temperature and pressure in a sonicator bath (37 kHz) for 24 h (see Experimental Section for details). This approach has extensively been employed to maximize the loading of carboxylic acid groups at the outer surface of CNTs, thus enhancing their hydrophilic character. If the latter feature is frequently invoked as a key pre-requisite of carbon-based nanomaterial as electrocatalysts in water-based electrolytes^[36], recent work by our group has unveiled that carboxylic acid groups do not generate the ideal electronic microenvironment to promote the 2e⁻ ORR efficiently^[25]. Despite the authors' awareness of the often batch-dependent nature of CNT samples prepared through straightforward bottom-up oxidation methods - as well as the limited control over the chemical composition and loading of oxygen-containing functional groups in the oxidized nanomaterials - we compared these preliminary, mild oxidation conditions with more severe ones. This comparison was made without overlooking the reproducibility of newly oxidized batches and their ultimate electrocatalytic performance in the ORR. The aim was to select the most appropriate batch conditions for a practical and easily scalable production of oxidized CNT samples featuring an optimal balance between loading and chemical identity of surface O-containing groups thus creating ideal surface microenvironments to boost the metal-free 2e⁻ ORR selectively. To this aim a second oxidized C-sample [MW-ox^{HT} (2)] was prepared without the aid of ultrasounds (that are known to maximize O-content)^[37] by refluxing overnight a CNT dispersion in *aqua regia*. A similar treatment of CNTs has already been reported in the literature but at room temperature with the production of only moderately wettable oxidized-CNTs samples^[28].

The two oxidized samples have been thoroughly characterized before being employed as electrocatalysts for the 2e⁻ ORR. From a morphological viewpoint, TEM images recorded from evaporative casting of alcoholic suspensions of MW-ox^{RT} (1) and MW-ox^{HT} (2) do not show relevant difference [Supplementary Figure 1],

except for a superior aggregation degree of C-flakes in MW-ox^{HT} (2). This is in accord with the lower oxidation degree measured in 2 (*vide infra*). Nitrogen physisorption analyses were carried out on the MWCNT sample before and after both oxidation protocols. Samples SSA showed largely superimposable BET profiles with only minor alterations of total pore volumes [p-MWCNTs 183 m²/g and 0.94 cm³/g; MW-ox^{RT} (1) 203 m²/g and 0.95 cm³/g; MW-ox^{HT} (2) 190 m²/g and 1.06 cm³/g]. All materials exhibit type IV isotherms featured by small H₂ hysteresis loops in the 0.8 ÷ 1.0 p/p⁰ range typical of mesoporous networks [Figure 1A and Supplementary Figure 2]^[38]. Pore size distribution analyses confirm the dominant mesoporous nature of both the oxidized samples with only p-MWCNTs exhibiting larger macropores (inset of Figure 1A and Supplementary Figure 2). In particular, MW-ox^{RT} (1) and MW-ox^{HT} (2) show prevalently mesopores in the 20-50 nm range, while pristine MWCNTs are characterized by larger pores spanning from mesopores (20-50 nm) till macropores (50-180 nm). The first evidence of MWCNT oxidation is provided by FT-IR spectroscopy. As shown in Supplementary Figure 3, the intensity ratio between vibrational signals in the 1,600-1,700 cm⁻¹ range - commonly ascribed to C=O stretching (ν)^[39] - and those typical of CNTs footprint in the 750-1,250 cm⁻¹ range^[39,40] are appreciably higher in 1 and 2 with respect to their pristine counterpart (MWCNTs). A similar trend is observed for the signals at ~3,400 cm⁻¹ associated with -OH stretching modes; despite the largely qualitative character of this poorly distinctive IR region, the higher relative intensity of the -OH band in 1 and 2 is coherent with the oxidation of the CNT surface.

Raman spectroscopy carried out on samples 1 and 2 reflects their different oxidation degree. As Supplementary Figure 4 shows, both oxidized samples exhibit higher intensity ratios of D and G modes (I_D/I_G) compared with their pristine counterpart (MWCNTs). This evidence is classically invoked as a distinctive feature of an increased materials surface defectivity as a consequence of the oxidation treatment each sample underwent. In this regard, the higher I_D/I_G ratio measured for 1 is in line with its deeper oxidation degree with respect to sample 2 (*vide infra*).

TGA, EA and high-resolution O 1s XPS spectroscopy have finally been employed to get more details on the chemico-physical composition of 1 and 2. Comparative TGA profiles of pristine MWCNTs along with those of oxidized samples 1 and 2 are provided on Figure 1B. Both oxidized samples show distinctive weight losses ascribed to the presence of thermally labile O-containing functionalities. This comparative analysis also highlights the significant gap between the two oxidized samples in terms of surface loading of O-containing functional groups as a consequence of the different oxidation protocols to get 1 and 2. Accordingly, 1 exhibits a markedly superior weight loss in the 40-750 °C thermal region compared to sample 2 thus confirming the superior ability of sulfo-nitric acid mixture to deeply oxidize nanocarbon materials already under mild (r.t.) temperature conditions^[27,28]. The different functionalization degrees of samples 1 and 2 have also been confirmed by EA and XPS analyses [Supplementary Table 1]. EAs clearly indicate a lower C-content in MW-ox^{RT} (1) with respect to MW-ox^{HT} (2), thus indirectly pointing out the superior oxidation degree of the former sample. On the same ground, XPS survey spectra [Supplementary Figure 5] show a lower C/O signals ratio in 1 vs. 2. To investigate the nature of O-containing groups in the oxidized materials, high resolution O 1s XPS signals were deconvoluted into three main components: 531.3 ± 0.2, 532.3 ± 0.2 and 533.1 ± 0.2 eV ascribed to carbonyl, carboxylic acids and C-OH groups (from carboxylic acids and phenols), respectively^[25,41,42]. As shown in Figure 1C and summarized in Supplementary Table 1, MW-ox^{RT} (1) presents a markedly high content of carboxylic groups (> 50%). On the other hand, the oxidation treatment at higher temperature values with *aqua regia* gives rise to materials oxidized at a lower extent but featuring a higher percentage of phenol-like moieties [Figure 1D and Supplementary Table 1]. A minor O 1s XPS component at 534.7 eV in 1 is finally ascribed to adventitious water^[43] [Figure 1C], as a consequence of the superior hydrophilic character of this highly oxidized sample.

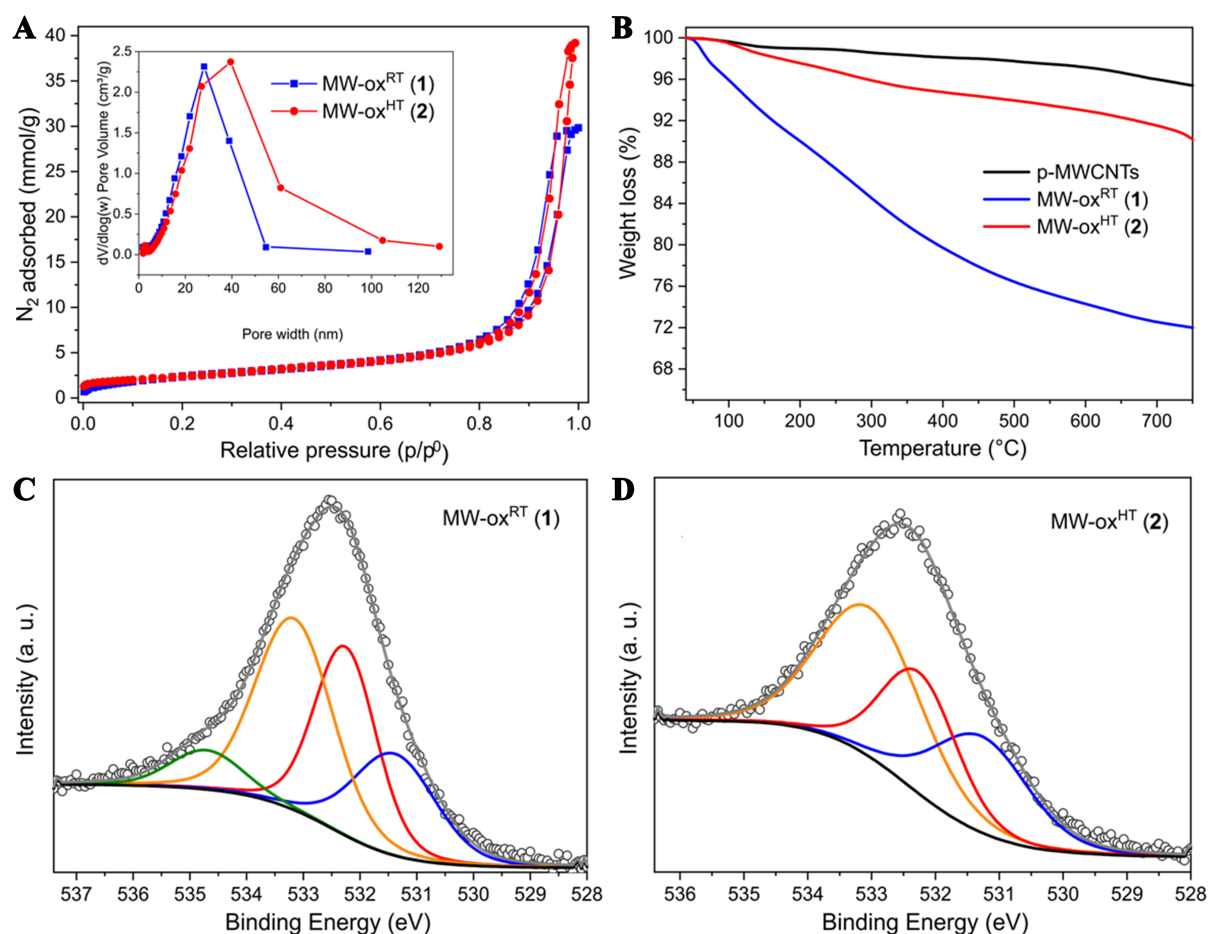


Figure 1. (A) N₂ adsorption-desorption isothermal curves conducted at 77 K for MW-ox^{RT} (1) and MW-ox^{HT} (2) along with their corresponding pore size distribution (inset); (B) TGA conducted on MW-ox^{RT} (1) and MW-ox^{HT} (2) in comparison with their pristine counterpart. Analyses conditions: from 40 to 750 °C (5 °C/min) in N₂ atmosphere (100 mL/min); (C) High-resolution O 1s XPS signal of MW-ox^{RT} (1) and (D) MW-ox^{HT} (2) along with their fitting deconvolution. TGA: Thermogravimetric analysis; XPS: X-ray photoelectron spectroscopy.

Electrocatalytic study of 1 and 2 in the 2e⁻ ORR

MW-ox^{RT} (1) and MW-ox^{HT} (2) have been tested as electrocatalysts for the selective 2e⁻ ORR to hydrogen peroxide. To this aim, all powdery C-based samples were dispersed upon sonication in a water/alcohol/Nafion® solution before being drop cast on a GC disk of the RRDE and left to evaporate at ambient conditions to get ultra-thin C-coatings (working electrode, see Experimental part for details). Electrochemical measurements were then carried out in an O₂-saturated alkaline solution using a three electrodes cell including - other than the working electrode - a Pt wire and an Ag/AgCl/KCl_{sat.} as counter and reference electrodes, respectively.

Qualitative evidence of the materials activity in ORR has first been achieved from cyclic voltametric tests. As shown in [Supplementary Figure 6](#) and [Figure 2A](#), both samples exhibit a well-defined reduction peak under O₂-saturated conditions not observed in N₂-saturated environments. Linear sweep voltammograms (LSV) have finally been acquired in the +0.1 ÷ -0.9 V range at an electrode spin rate of 900 rpm to get further details on the ORR activity of oxidized samples 1 and 2 along with that of their pristine counterpart (MWCNTs). Background currents measured under saturated N₂ conditions were then subtracted from each curve to eliminate the capacitive contributions. As shown in [Figure 2B\(i\)](#), both oxidized materials display

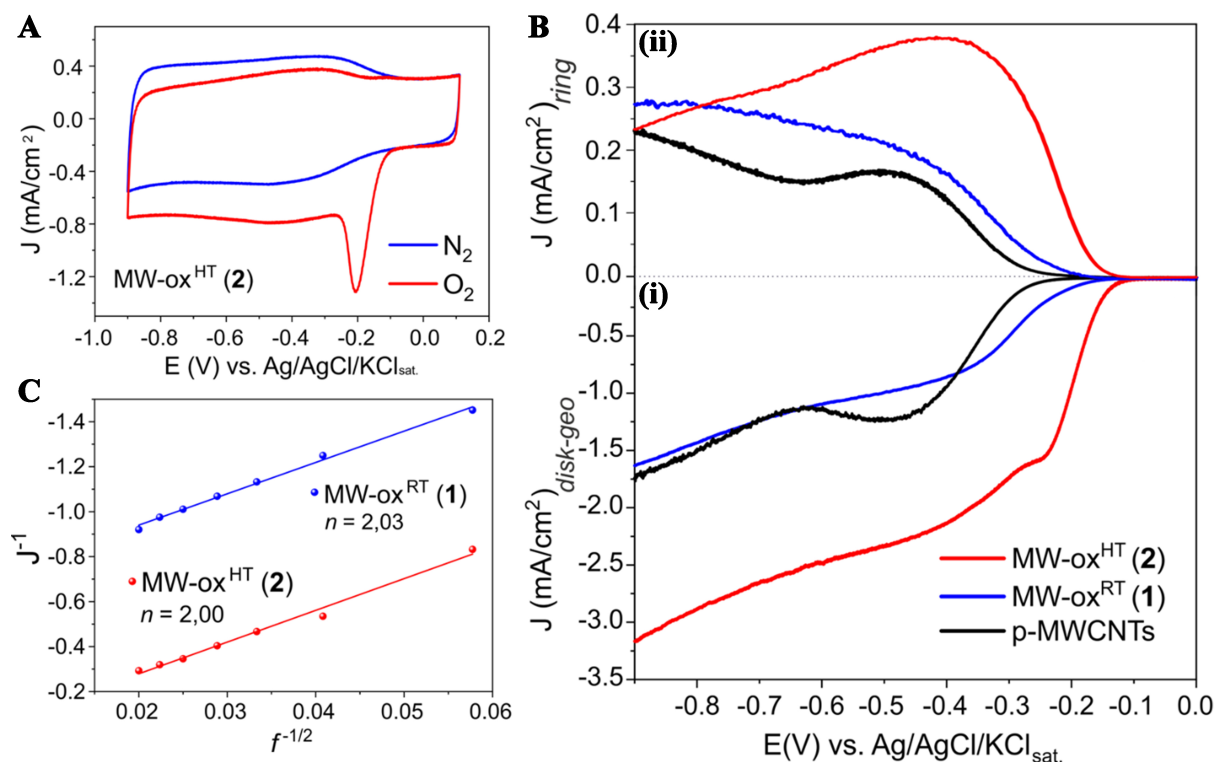


Figure 2. (A) CV acquired in N₂ and O₂ saturated KOH 0.1 M solution for MW-ox^{HT} (2) at 10 mV/s in the +0.1 ÷ -0.9 V vs. Ag/AgCl/KCl_{sat.} potential range; [B(i)] LSV curves acquired for p-MWCNTs, MW-ox^{RT} (1) and MW-ox^{HT} (2) in O₂-saturated KOH 0.1 M solution at 900 rpm at the GC disk electrode and [B(ii)] correspondent curves registered at the Pt-ring electrode; (C) K-L plot of MW-ox^{RT} (1) and MW-ox^{HT} (2) extrapolated from respective LSV curves at -0.4 V. CV: Cyclic voltammograms; LSV: linear sweep voltammograms; MWCNTs: multi-walled carbon nanotubes; GC: glassy carbon.

positive onset overpotential shifts compared with pristine MWCNTs. In particular, MW-ox^{HT} (2) shows an onset value of -0.14 V vs. Ag/AgCl/KCl_{sat.} [Table 1], with a remarkable overpotential shift of about +160 mV with respect to pristine MWCNTs.

In addition to a markedly low onset potential value, MW-ox^{HT} (2) exhibits a pretty high Pt-ring current density [Figure 2B(ii)] directly related to the amount of hydrogen peroxide produced. As a matter of fact, a 2e⁻ dioxygen reduction pathway with a selectivity up to 85% [Table 1 and Supplementary Figure 7A] is observed with this oxidized material at work. In spite of an equally high selectivity of 1 towards H₂O₂, the markedly lower current density and the worse onset potential value (-0.20 V) of this electrocatalyst, make it a less attractive material for the selective 2e⁻ ORR [Table 1]. The Koutecky-Levich equation has finally been applied to measure the average number of electrons transferred per O₂ molecule (*n*) with the two electrocatalysts at comparison. To this end, LSV curves of each sample have been recorded at different electrode spin rates (from 300 to 2,500 rpm, Supplementary Figure 8) and the corresponding K-L plots have traced out [Figure 2C]. Apart from the limits of analytical methods applied to the quantification of H₂O₂ [44], K-L plots have confirmed the ability of both oxidized samples to foster a prevalent 2e⁻ transfer process, typical of a chemoselective O₂ reduction path to hydrogen peroxide [Table 1 and Supplementary Figure 7B]. As mentioned above, MW-ox^{HT} (2) also presents a net superior current density with respect to MW-ox^{RT} (1) counterpart as confirmed by the higher half-wave potential value of the former [Figure 2B(i) and Table 1]. As a consequence, the H₂O₂ mass activity expressed as mA per mg_{CAT} is more than doubled in 2 vs. 1 and/or their pristine counterpart MWCNTs [Table 1]. Tafel analysis further confirms the superior catalytic activity

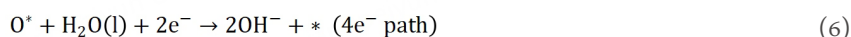
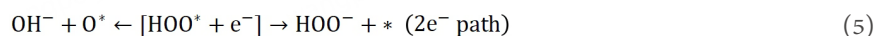
Table 1. Onset and half-wave potential values, H₂O₂%, average number of exchanged electrons (*n*) per O₂ molecule and mass activity measured for p-MWCNTs, MW-ox^{RT} (1) and MW-ox^{HT} (2)

Sample	E _{ON} (V) ^a	E _{1/2} (V) ^a	H ₂ O ₂ (%) ^b	n _{K-L} ^c	Mass activity (mA/mg _{CAT}) ^d
p-MWCNTs	-0.30	-0.39	50	-	3.21
MW-ox ^{RT} (1)	-0.20	-0.38	87	2.03	2.93
MW-ox ^{HT} (2)	-0.14	-0.25	85	2.00	7.25

^aPotential values vs. Ag/AgCl/KCl_{sat.}; ^bH₂O₂% as calculated from the measured Pt-ring current of the RRDE at -0.4 V; ^caverage number of electrons exchanged per O₂ molecule as calculated from the K-L equation at -0.4 V; ^dmass activity as calculated from the ring curves of Figure 2B(ii) at -0.4 V. MWCNTs: Multi-walled carbon nanotubes; RRDE: rotating ring-disk electrode.

of MW-ox^{HT} (2). As illustrated in Supplementary Figure 9, 2 exhibits a significantly lower Tafel slope of 43 mV/dec, approximately half of the value registered for 1. Noteworthy, MW-ox^{HT} (2) ranks among the best performing O-doped carbon-based materials reported so far for the process [Supplementary Table 2]^[22,25,36,45-59].

Close selectivity values of the two oxidized samples led us to conclude that whatever the electrocatalyst at work (1 or 2), after dioxygen adsorption [Equation (3)] and the first proton-coupled electron transfer [Equation (4)], both materials bind the key intermediate HOO* weakly enough to allow its fast desorption [Equation (5), right-hand side] before O-O dissociation path [Equation (5), left-hand side and Equation (6)] takes place (competitive 4e⁻ ORR).



On the other hand, the superior mass-activity with 2 is basically attributed to unique surface chemico-physical properties of the sample, as the result of an unconventional and high-temperature oxidation treatment of MWCNTs with *aqua regia*. The lower oxidation degree (i.e., the reduced loading of O-containing functional groups), combined with the variable chemical composition of surface groups (i.e., phenolic vs. carboxylic groups), is supposed to generate an ideal and highly reproducible surface microenvironment for the efficient and low-overpotential activation/reduction of dioxygen.

Lastly, the net improvement of 2e⁻ ORR performance (activity and selectivity) measured in the sequence pristine MWCNTs vs. 1 vs. 2 [Table 1] demonstrate the key role of selected O-containing functionalities (i.e., phenol groups vs. carboxylic acids) on the electroreduction path, rather than the material oxidation degree. Neither a too high oxidation degree of the nanomaterial nor the presence of a relatively higher concentration of carboxylic acid at its outer surface [i.e., sulfo-nitric vs. chloro-nitric (*aqua regia*) oxidation method], seem to really control the 2e⁻ activation/reduction of dioxygen.

CONCLUSIONS

Two oxidized MWCNTs materials have been straightforwardly prepared using easily scalable and highly reproducible synthetic protocols. MW-ox^{RT} (1) and MW-ox^{HT} (2) isolated from the purification of MWCNT

suspensions in sulfo-nitric or chloro-nitric (*aqua regia*) mixtures, respectively, have been characterized with respect to their morphological and chemical composition before being tested as metal-free electrocatalysts for the challenging $2e^-$ ORR process. The sample prepared by the *aqua regia* oxidation method [MW-ox^{HT} (2)] has shown a minor surface oxidation degree and a higher enrichment in phenolic moieties. As a result, ORR starts on 2 already at -0.14 V vs. Ag/AgCl/KCl_{sat.} and its current density profile (J) exhibits a superior half-wave potential value compared to the overoxidized and carboxylic acids enriched MW-ox^{RT} (1) material. On the other hand, both oxidized samples show an almost complete selectivity towards the $2e^-$ ORR, indicating an equally fast desorption of the key HOO[•] reduction intermediate before undergoing the undesired O–O bond breaking ($4e^-$ reduction path). The net improvement of $2e^-$ ORR performance (activity and selectivity) measured in the sequence pristine MWCNTs vs. 1 vs. 2, is used to validate the role of selected O-containing functionalities in the electroreduction path (i.e., phenol groups vs. carboxylic acids), rather than that of material oxidation degree. Neither a too high oxidation degree of the nanomaterial nor the presence of a relatively higher concentration of carboxylic acids in MWCNTs [i.e., sulfo-nitric vs. chloro-nitric (*aqua regia*) oxidation method], can be claimed to control the $2e^-$ activation/reduction of dioxygen.

Guided by our results on $2e^-$ ORR promoted by tailored O-decorated carbon nanomaterials^[25], a facile, scalable and highly reproducible one-pot protocol has now been developed to generate moderately oxidized MWCNTs containing relatively high concentrations of surface phenolic groups. The latter have confirmed their key role in fostering the selective and efficient $2e^-$ reduction of dioxygen already under low overpotential values.

DECLARATIONS

Authors' contributions

Conceptualization: Tuci, G.; Bonechi, M.; Innocenti, M.; Giambastiani, G.

Methodology and its development: Tuci, G.; Giambastiani, G.

Validation: Tuci, G.; Giambastiani, G.; Bonechi, M.

Formal analysis: Tuci, G.; Bonechi, M.; Rossin, A.; Berretti, E.; Ceppatelli, M.; Poggini, L.

Investigation: Tuci, G.; Bonechi, M.

Data curation: Tuci, G.; Giambastiani, G.; Bonechi, M.; Innocenti, M.; Ceppatelli, M.

Writing - original draft: Tuci, G.; Giambastiani, G.; Bonechi, M.

Supervision: project management/coordination: Tuci, G.; Giambastiani, G.; Innocenti, M.

Funding acquisition: Tuci, G.; Giambastiani, G.; Innocenti, M.

Availability of data and materials

The raw data supporting the findings of this study are available within this Article and its [Supplementary Materials](#). Further data is available from the corresponding authors upon reasonable request.

Financial support and sponsorship

The authors would like to thank the Italian MUR through the PRIN2022 project “MATISSE - A ‘Molecular Lift’ for the Control of the Metal Protrusion and Coordination Sphere in Single-Atom Catalysts for CO₂ Electroreduction” (2022K5SX27) and the European Union - NextGeneration EU through the Italian Ministry of Environment and Energy Security POR H2 AdP MMES/ENEA with involvement of CNR and RSE, PNRR - Mission 2, Component 2, Investment 3.5 “Ricerca e sviluppo sull'idrogeno”, CUP: B93C22000630006 for financial support to this work. The financial support provided by the MUR - Dipartimenti di Eccellenza 2023-2027 (DICUS 2.0) to the Department of Chemistry “Ugo Schiff” of the University of Florence is also acknowledged. Acknowledgements are expressed to the European Union - NextGeneration EU for funding the project IPHOQS “Integrated Infrastructure Initiative in Photonic and

Quantum Sciences” - I-PHOQS [IR0000016, ID D2B8D520, CUP B53C22001750006] and the Circular and Sustainable Made in Italy Extended Partnership (MICS), Piano Nazionale di Ripresa e Resilienza (PNRR) - Missione 4, Componente 2, Investimento 1.3 - D.D. 1551.11-10-2022, PE00000004.

Conflicts of interest

Giambastiani, G. is Guest Editor of the Special Issue “Carbon in Catalysis” and Associate Editor of the journal *Chemical Synthesis*. Giambastiani, G. was not involved in any steps of editorial processing, notably including reviewers’ selection, manuscript handling, or decision-making. The other authors declare that there are no conflicts of interest.

Ethical approval and consent to participate

Not applicable.

Consent for publication

Not applicable.

Copyright

© The Author(s) 2025.

REFERENCES

1. Targhan, H.; Evans, P.; Bahrami, K. A review of the role of hydrogen peroxide in organic transformations. *J. Ind. Eng. Chem.* **2021**, *104*, 295-332. [DOI](#)
2. Fukuzumi, S.; Lee, Y.; Nam, W. Recent progress in production and usage of hydrogen peroxide. *Chin. J. Catal.* **2021**, *42*, 1241-52. [DOI](#)
3. Lee, K.; Lim, J.; Lee, M. J.; et al. Structure-controlled graphene electrocatalysts for high-performance H₂O₂ production. *Energy. Environ. Sci.* **2022**, *15*, 2858-66. [DOI](#)
4. Campos-Martin, J. M.; Blanco-Brieva, G.; Fierro, J. L. Hydrogen peroxide synthesis: an outlook beyond the anthraquinone process. *Angew. Chem. Int. Ed. Engl.* **2006**, *45*, 6962-84. [DOI](#) [PubMed](#)
5. Yang, S.; Verdaguer-Casadevall, A.; Arnarson, L.; et al. Toward the decentralized electrochemical production of H₂O₂: a focus on the catalysis. *ACS. Catal.* **2018**, *8*, 4064-81. [DOI](#)
6. Perry, S. C.; Pangotra, D.; Vieira, L.; et al. Electrochemical synthesis of hydrogen peroxide from water and oxygen. *Nat. Rev. Chem.* **2019**, *3*, 442-58. [DOI](#)
7. Pang, Y.; Xie, H.; Sun, Y.; Titirici, M.; Chai, G. Electrochemical oxygen reduction for H₂O₂ production: catalysts, pH effects and mechanisms. *J. Mater. Chem. A.* **2020**, *8*, 24996-5016. [DOI](#)
8. Zhang, Y. L.; Goh, K.; Zhao, L.; et al. Advanced non-noble materials in bifunctional catalysts for ORR and OER toward aqueous metal-air batteries. *Nanoscale* **2020**, *12*, 21534-59. [DOI](#)
9. Li, Y.; Li, Q.; Wang, H.; Zhang, L.; Wilkinson, D. P.; Zhang, J. Recent progresses in oxygen reduction reaction electrocatalysts for electrochemical energy applications. *Electrochem. Energ. Rev.* **2019**, *2*, 518-38. [DOI](#)
10. Papanikolaou, G.; Centi, G.; Perathoner, S.; Lanzafame, P. Catalysis for e-chemistry: need and gaps for a future de-fossilized chemical production, with focus on the role of complex (direct) syntheses by electrocatalysis. *ACS. Catal.* **2022**, *12*, 2861-76. [DOI](#) [PubMed](#) [PMC](#)
11. Verdaguer-Casadevall, A.; Deiana, D.; Karamad, M.; et al. Trends in the electrochemical synthesis of H₂O₂: enhancing activity and selectivity by electrocatalytic site engineering. *Nano. Lett.* **2014**, *14*, 1603-8. [DOI](#)
12. Jirkovský, J. S.; Panas, I.; Ahlberg, E.; Halasa, M.; Romani, S.; Schiffrin, D. J. Single atom hot-spots at Au-Pd nanoalloys for electrocatalytic H₂O₂ production. *J. Am. Chem. Soc.* **2011**, *133*, 19432-41. [DOI](#) [PubMed](#)
13. Wu, S.; Yu, L.; Wen, G.; Xie, Z.; Lin, Y. Recent progress of carbon-based metal-free materials in thermal-driven catalysis. *J. Energy. Chem.* **2021**, *58*, 318-35. [DOI](#)
14. Jaryal, V. B.; Villa, A.; Gupta, N. Metal-free carbon-based nanomaterials: insights from synthesis to applications in sustainable catalysis. *ACS. Sustainable. Chem. Eng.* **2023**, *11*, 14841-65. [DOI](#)
15. Tuci, G.; Pilaski, M.; Ba, H.; et al. Unraveling surface basicity and bulk morphology relationship on covalent triazine frameworks with unique catalytic and gas adsorption properties. *Adv. Funct. Mater.* **2017**, *27*, 1605672. [DOI](#)
16. Yang, L.; Shui, J.; Du, L.; et al. Carbon-based metal-free ORR electrocatalysts for fuel cells: past, present, and future. *Adv. Mater.* **2019**, *31*, e1804799. [DOI](#)
17. Li, Y.; Tong, Y.; Peng, F. Metal-free carbocatalysis for electrochemical oxygen reduction reaction: activity origin and mechanism. *J.*

- Energy. Chem.* **2020**, *48*, 308–21. DOI
18. He, H.; Liu, S.; Liu, Y.; et al. Review and perspectives on carbon-based electrocatalysts for the production of H₂O₂ via two-electron oxygen reduction. *Green. Chem.* **2023**, *25*, 9501–42. DOI
 19. Sang, Z.; Hou, F.; Wang, S.; Liang, J. Research progress on carbon-based non-metallic nanomaterials as catalysts for the two-electron oxygen reduction for hydrogen peroxide production. *New. Carbon. Mater.* **2022**, *37*, 136–51. DOI
 20. Zhou, W.; Xie, L.; Gao, J.; et al. Selective H₂O₂ electrosynthesis by O-doped and transition-metal-O-doped carbon cathodes via O₂ electroreduction: a critical review. *Chem. Eng. J.* **2021**, *410*, 128368. DOI
 21. Shen, X.; Wang, Z.; Guo, H.; Lei, Z.; Liu, Z.; Wang, L. Solvent engineering of oxygen-enriched carbon dots for efficient electrochemical hydrogen peroxide production. *Small* **2023**, *19*, e2303156. DOI PubMed
 22. Sun, F.; Yang, C.; Qu, Z.; et al. Inexpensive activated coke electrocatalyst for high-efficiency hydrogen peroxide production: coupling effects of amorphous carbon cluster and oxygen dopant. *Appl. Catal. B. Environ.* **2021**, *286*, 119860. DOI
 23. Zhang, D.; Tsounis, C.; Ma, Z.; et al. Highly selective metal-free electrochemical production of hydrogen peroxide on functionalized vertical graphene edges. *Small* **2022**, *18*, e2105082. DOI PubMed
 24. Tuci, G.; Rossin, A.; Saki, Z.; et al. The still elusive role of lightweight doping in carbon-based electrocatalysts for the selective oxygen reduction reaction to hydrogen peroxide. *ChemSusChem* **2024**, *17*, e202400660. DOI PubMed
 25. Tuci, G.; Rossin, A.; Zhang, X.; et al. Metal-free electrocatalysts for the selective 2e[−] oxygen reduction reaction: a never-ending story? *Chemistry* **2023**, *29*, e202301036. DOI PubMed
 26. Tuci, G.; Rossin, A.; Zhang, X.; Pham-Huu, C.; Giambastiani, G. Exohedrally functionalized carbon-based networks as catalysts for electrochemical syntheses. *Curr. Opin. Green. Sustain. Chem.* **2022**, *33*, 100579. DOI
 27. Samori, C.; Sainz, R.; Ménard-Moyon, C.; et al. Potentiometric titration as a straightforward method to assess the number of functional groups on shortened carbon nanotubes. *Carbon* **2010**, *48*, 2447–54. DOI
 28. Lavagna, L.; Bartoli, M.; Suarez-Riera, D.; Cagliero, D.; Musso, S.; Pavese, M. Oxidation of carbon nanotubes for improving the mechanical and electrical properties of oil-well cement-based composites. *ACS. Appl. Nano. Mater.* **2022**, *5*, 6671–8. DOI
 29. Fairley, N.; Fernandez, V.; Richard-Plouet, M.; et al. Systematic and collaborative approach to problem solving using X-ray photoelectron spectroscopy. *Appl. Surf. Sci. Adv.* **2021**, *5*, 100112. DOI
 30. Ceppatelli, M.; Gorelli, F. A.; Haines, J.; Santoro, M.; Bini, R. Probing high-pressure reactions in heterogeneous materials by Raman spectroscopy. *Z. Kristallogr.* **2014**, *229*, 83–91. DOI
 31. Ferrari, A. C.; Robertson, J. Interpretation of Raman spectra of disordered and amorphous carbon. *Phys. Rev. B.* **2000**, *61*, 14095–107. DOI
 32. Ferrari, A. C.; Robertson, J. Resonant Raman spectroscopy of disordered, amorphous, and diamondlike carbon. *Phys. Rev. B.* **2001**, *64*, 075414. DOI
 33. Lucchese, M.; Stavale, F.; Ferreira, E. M.; et al. Quantifying ion-induced defects and Raman relaxation length in graphene. *Carbon* **2010**, *48*, 1592–7. DOI
 34. Wang, Y.; Zhang, D.; Liu, H. A study of the catalysis of cobalt hydroxide towards the oxygen reduction in alkaline media. *J. Power. Sources.* **2010**, *195*, 3135–9. DOI
 35. Chen, Y.; Wang, S.; Li, Z. A cobalt-pyrrole coordination compound as high performance cathode catalyst for direct borohydride fuel cells. *RSC. Adv.* **2020**, *10*, 29119–27. DOI PubMed PMC
 36. Dong, K.; Liang, J.; Wang, Y.; et al. Honeycomb carbon nanofibers: a superhydrophilic O₂-entrapping electrocatalyst enables ultrahigh mass activity for the two-electron oxygen reduction reaction. *Angew. Chem. Int. Ed. Engl.* **2021**, *60*, 10583–7. DOI PubMed
 37. Jun, L. Y.; Mubarak, N.; Yon, L. S.; Bing, C. H.; Khalid, M.; Abdullah, E. Comparative study of acid functionalization of carbon nanotube via ultrasonic and reflux mechanism. *J. Environ. Chem. Eng.* **2018**, *6*, 5889–96. DOI
 38. Aranovich, G.; Donohue, M. Analysis of adsorption isotherms: lattice theory predictions, classification of isotherms for gas–solid equilibria, and similarities in gas and liquid adsorption behavior. *J. Colloid. Interface. Sci.* **1998**, *200*, 273–90. DOI
 39. de Menezes, B. R. C.; Ferreira, F. V.; Silva, B. C.; et al. Effects of octadecylamine functionalization of carbon nanotubes on dispersion, polarity, and mechanical properties of CNT/HDPE nanocomposites. *J. Mater. Sci.* **2018**, *53*, 14311–27. DOI
 40. Mishra, S. K.; Tripathi, S. N.; Choudhary, V.; Gupta, B. D. Surface plasmon resonance-based fiber optic methane gas sensor utilizing graphene-carbon nanotubes-poly(methyl methacrylate) hybrid nanocomposite. *Plasmonics* **2015**, *10*, 1147–57. DOI
 41. Yu, B.; Wang, X.; Qian, X.; et al. Functionalized graphene oxide/phosphoramidate oligomer hybrids flame retardant prepared via in situ polymerization for improving the fire safety of polypropylene. *RSC. Adv.* **2014**, *4*, 31782. DOI
 42. Stevens, J. S.; Seabourne, C. R.; Jaye, C.; Fischer, D. A.; Scott, A. J.; Schroeder, S. L. Incisive probing of intermolecular interactions in molecular crystals: core level spectroscopy combined with density functional theory. *J. Phys. Chem. B.* **2014**, *118*, 12121–9. DOI PubMed
 43. Rojas, J.; Toro-Gonzalez, M.; Molina-Higgins, M.; Castano, C. Facile radiolytic synthesis of ruthenium nanoparticles on graphene oxide and carbon nanotubes. *Mater. Sci. Eng. B.* **2016**, *205*, 28–35. DOI
 44. Zhou, R.; Zheng, Y.; Jaroniec, M.; Qiao, S. Determination of the electron transfer number for the oxygen reduction reaction: from theory to experiment. *ACS. Catal.* **2016**, *6*, 4720–8. DOI
 45. Lu, Z.; Chen, G.; Siahrostami, S.; et al. High-efficiency oxygen reduction to hydrogen peroxide catalysed by oxidized carbon materials. *Nat. Catal.* **2018**, *1*, 156–62. DOI
 46. Kim, H. W.; Ross, M. B.; Kornienko, N.; et al. Efficient hydrogen peroxide generation using reduced graphene oxide-based oxygen

- reduction electrocatalysts. *Nat. Catal.* **2018**, *1*, 282-90. DOI
47. Han, G. F.; Li, F.; Zou, W.; et al. Building and identifying highly active oxygenated groups in carbon materials for oxygen reduction to H₂O₂. *Nat. Commun.* **2020**, *11*, 2209. DOI PubMed PMC
48. San Roman, D.; Krishnamurthy, D.; Garg, R.; et al. Engineering three-dimensional (3D) out-of-plane graphene edge sites for highly selective two-electron oxygen reduction electrocatalysis. *ACS. Catal.* **2020**, *10*, 1993-2008. DOI
49. Pang, Y.; Wang, K.; Xie, H.; Sun, Y.; Titirici, M.; Chai, G. Mesoporous carbon hollow spheres as efficient electrocatalysts for oxygen reduction to hydrogen peroxide in neutral electrolytes. *ACS. Catal.* **2020**, *10*, 7434-42. DOI
50. Chen, S.; Luo, T.; Chen, K.; et al. Chemical identification of catalytically active sites on oxygen-doped carbon nanosheet to decipher the high activity for electro-synthesis hydrogen peroxide. *Angew. Chem. Int. Ed. Engl.* **2021**, *60*, 16607-14. DOI PubMed
51. Lee, J.; Lee, Y.; Lim, J. S.; et al. Discriminating active sites for the electrochemical synthesis of H₂O₂ by molecular functionalisation of carbon nanotubes. *Nanoscale* **2022**, *15*, 195-203. DOI PubMed
52. Wang, W.; Hu, Y.; Liu, Y.; Zheng, Z.; Chen, S. Self-powered and highly efficient production of H₂O₂ through a Zn-air battery with oxygenated carbon electrocatalyst. *ACS. Appl. Mater. Interfaces.* **2018**, *10*, 31855-9. DOI PubMed
53. Zhang, H.; Li, Y.; Zhao, Y.; Li, G.; Zhang, F. Carbon black oxidized by air calcination for enhanced H₂O₂ generation and effective organics degradation. *ACS. Appl. Mater. Interfaces.* **2019**, *11*, 27846-53. DOI PubMed
54. Zhu, J.; Xiao, X.; Zheng, K.; et al. KOH-treated reduced graphene oxide: 100% selectivity for H₂O₂ electroproduction. *Carbon* **2019**, *153*, 6-11. DOI
55. Sa, Y. J.; Kim, J. H.; Joo, S. H. Active edge-site-rich carbon nanocatalysts with enhanced electron transfer for efficient electrochemical hydrogen peroxide production. *Angew. Chem. Int. Ed. Engl.* **2019**, *58*, 1100-5. DOI PubMed
56. Lim, J. S.; Kim, J. H.; Woo, J.; et al. Designing highly active nanoporous carbon H₂O₂ production electrocatalysts through active site identification. *Chem* **2021**, *7*, 3114-30. DOI
57. She, F.; Guo, Z.; Liu, F.; et al. Curvature-dependent electrochemical hydrogen peroxide synthesis performance of oxidized carbon nanotubes. *ACS. Catal.* **2024**, *14*, 10928-38. DOI
58. Xing, Z.; Shi, K.; Parsons, Z. S.; Feng, X. Interplay of active sites and microenvironment in high-rate electrosynthesis of H₂O₂ on doped carbon. *ACS. Catal.* **2023**, *13*, 2780-9. DOI
59. Guo, Y.; Zhang, R.; Zhang, S.; et al. Ultrahigh oxygen-doped carbon quantum dots for highly efficient H₂O₂ production via two-electron electrochemical oxygen reduction. *Energy. Environ. Sci.* **2022**, *15*, 4167-74. DOI